

# Electronic communication between Co and Ru sites decorated on nitrogen-doped carbon nanotubes boost the alkaline hydrogen evolution reaction

Mengting Gao,<sup>a,#</sup> Ying Wei,<sup>a,#</sup> Xuemeng Huo,<sup>a</sup> Wenjie Zhu,<sup>a</sup> Qingqing Liu,<sup>a</sup> Jinyuan Qiang,<sup>a</sup> Wanwan Liu,<sup>a</sup> Ying Wang,<sup>a</sup> Xu Li,<sup>a</sup> Jianfeng Huang,<sup>a</sup> Yongqiang Feng<sup>a,\*</sup>

<sup>a</sup> School of Materials Science and Engineering, Shaanxi University of Science and Technology, Xi'an 710021, China

E-mail: fengyq@sust.edu.cn

# these authors contribute equally to this work

**Keywords:** CoRu alloy • electrocatalyst • water splitting • hydrogen evolution reaction • carbon nanotubes

**Abstract:** Designing highly efficient Pt-free electrocatalysts with low overpotential for the alkaline hydrogen evolution reaction (HER) remains a significant challenge. Here, a novel and efficient Co, Ru bimetallic electrocatalyst composed by CoRu nanoalloy decorated on the N-doped carbon nanotubes (N-CNTs), deriving from the fullerene and melamine via hydrothermal treatment followed by pyrolysis. Benefiting from the electronic communication between Co and Ru sites, the as-obtained CoRu@N-CNTs exhibited superior electrocatalytic HER activity. To deliver a current density of 10 mA cm<sup>-2</sup>, it required an overpotential of merely 19 mV along with a Tafel slope of 26.19 mV dec<sup>-1</sup> in 1 M KOH, outperforming the benchmark Pt/C catalyst. The present work would pave a new way for the design and construction of efficient electrocatalyst for energy storage and conversion.

## 1. Introduction

A viable approach to addressing both the direct energy deficit and the greenhouse effect is electrocatalytic water splitting, which is a significant way to manufacture hydrogen (H<sub>2</sub>) on a big scale and at a low cost [1-6]. In the overall water splitting process, the electrochemical hydrogen evolution reaction (HER) presents an alluring approach to producing H<sub>2</sub> as one of the most promising substitutes for traditional fossil fuels [7-9]. Currently, noble metal Pt and/or Pt-based catalysts are extensively utilized as electrocatalysts for HER. Nevertheless, their exorbitant expense and restricted accessibility impede their widespread practical application [10-13]. Therefore, a formidable task is to find effective Pt-free electrocatalysts for HER.

Ru, the most inexpensive noble metal, has emerged as the preferred substitute for Pt due to its medium-strength bond with hydrogen (about 65 kcal mol<sup>-1</sup>) and its cost, which is only one-third of Pt. The inherent activity of Ru for alkaline HER is, however, greatly diminished by its restricted capacity to adsorb and dissociate H<sub>2</sub>O [14-17]. There are two primary factors that contribute to the enhancement of catalytic activity for Ru: (1)

Increasing the number of attainable active sites, which can be achieved by enlarging the specific surface area of the catalyst materials [18-22]. Generally, dispersing noble-metals on supports with high surface areas is an attractive approach to increase the number of active sites and then improve the catalytic activity [23]. (2) Improving the intrinsic activity, which is commonly accomplished by complicated structure/composition hybridization and electronic property tuning [13, 24-26]. The chemical and electrical characteristics of Ru can be readily changed by heteroatom bond formation, improving its suitability for electrocatalytic HER [27-29]. Recently, a great deal of research has been done on diatomic catalysts (DAC), which combine to increase intrinsic activity by controlling the adsorption and desorption capacities of various metals [30-33]. The adsorption capability of the catalyst on active sites can be greatly enhanced by the action of neighboring metal atoms in DAC on the surrounding electronic environment [34, 35].

Herein, a novel and efficient Co, Ru bimetallic electrocatalyst composed by CoRu nanoalloy decorated on the N-doped carbon nanotubes (N-CNTs), deriving from the fullerene (C<sub>60</sub>(OH)<sub>n</sub>) and melamine via hydrothermal treatment followed with pyrolysis. The presence of Co catalyzed fullerene and melamine into N-CNTs, which could serve as electron collector. Benefiting from the strong electronic communication between Co and Ru moiety, the as-obtained CoRu@N-CNTs exhibited outperforming electrocatalytic HER activity. To deliver a current density of 10 mA cm<sup>-2</sup>, it required an overpotential of merely 19 mV along with a Tafel slope of 26.19 mV dec<sup>-1</sup> in 1 M KOH. The present work provided a new clue for design and construction of efficient HER electrocatalyst.

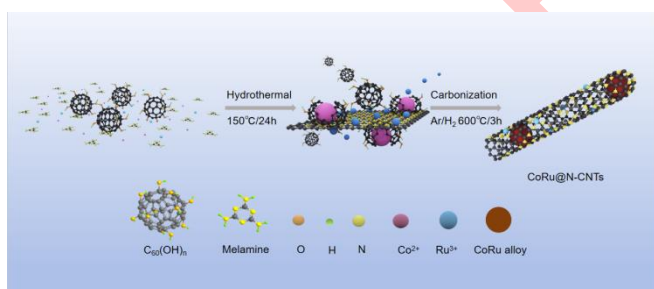
## 2. Experimental Section

### 2.1. Materials

1 Cobalt(II) chloride ( $\text{CoCl}_2$ ), ethanol ( $\text{EtOH}$ ,  $\text{CH}_3\text{CH}_2\text{OH}$ )  
 2 isopropyl alcohol (IPA,  $\text{C}_3\text{H}_8\text{O}$ ) were purchased from Sinopharm  
 3 Chemical Reagent Co., Ltd. Ruthenium (III) chloride anhydrous  
 4 ( $\text{RuCl}_3$ ), platinum on activated carbon (20 wt% Pt/C), Nafion  
 5 solution (5%) and potassium hydroxide ( $\text{KOH}$ , 1.0 M) were  
 6 purchased from Sigma-Aldrich, deionized (DI) water (resistivity:  
 7  $\geq 18.25 \text{ M}\Omega\cdot\text{cm}$ ) was provided by an ultrapure water system  
 8 (ULUPURE, UPDR-I-10 T). All the chemicals are analytical  
 9 grade and used directly without further treatment.

## 10 2.2. Synthesis of CoRu@N-CNTs

11 The preparation procedure of CoRu@N-CNTs was  
 12 schematically illustrated in Scheme 1. Briefly, 1.2 g of melamine,  
 13 150 mg of  $\text{C}_{60}(\text{OH})_n$ , 0.5 mmol of  $\text{CoCl}_2$  and 0.5 mmol of  $\text{RuCl}_3$   
 14 were dissolved into 70 ml of deionized water. The mixture  
 15 solution was then transferred to a stainless-steel capped Teflon  
 16 autoclave. After hydrothermal treatment at  $150^\circ\text{C}$  for 24 h, the  
 17 solid precursor of CoRu@N-CNTs was obtained by extraction  
 18 filtration. Then the obtained powder was carbonized in a tube  
 19 furnace under  $\text{Ar}/\text{H}_2$  (5%) flow for 3 h at  $600^\circ\text{C}$  with a raising  
 20 rate of  $5^\circ\text{C min}^{-1}$ . After cooling naturally to the room  
 21 temperature, the CoRu@N-CNTs was successfully prepared.  
 22 For comparison, CoRu@NC, Co@N-CNTs and Ru@NC were  
 23 also prepared following a similar procedure to CoRu@N-CNTs  
 24 except in the absence of  $\text{C}_{60}(\text{OH})_n$ ,  $\text{RuCl}_3$  and  $\text{CoCl}_2$ ,  
 25 respectively. For detail, please see in the Supporting Information.



27 **Scheme 1.** Schematic illustration for the synthesis process of CoRu@N-CNTs.

## 28 2.3. Material characterization

29 The X-ray diffraction (XRD) were recorded on a Rigaku  
 30 D/max-2200PC diffractometer (Japan) using  $\text{Cu K}\alpha$  radiation.  
 31 Raman spectra were conducted on a Renishaw-invia  
 32 microscopic confocal laser Raman spectrometer with 532 nm as  
 33 the excitation laser. The morphology of the samples was tested  
 34 using a field-emission scanning electron microscope (SEM,  
 35 Hitachi S-4800). The microstructure and elemental mapping  
 36 analysis of the samples were investigated by transmission  
 37 electron microscopy (TEM) exerted on a FEI Tecnai G2 F20 S-  
 38 TWIN instrument. X-ray photoelectron spectroscopy (XPS) were  
 39 recorded on the Thermo Scientific ESCA Lab 250Xi with 200 W  
 40 monochromated  $\text{Al K}\alpha$  radiation. All the electrochemical  
 41 performance was tested on a CHI 660E workstation (Chenhua,  
 42 Shanghai).

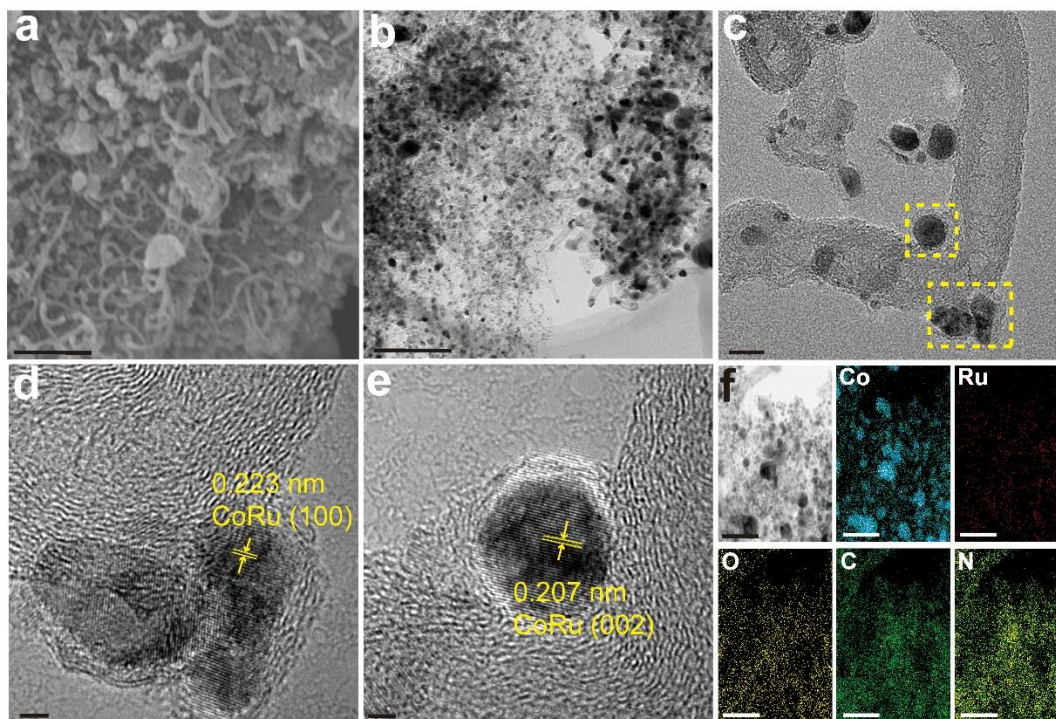
## 43 2.4. Electrochemical measurement

The HER test was performed on the electrochemical  
 workstation (CHI 660E, Chenhua, Shanghai) using a three-  
 electrode system in Ar-saturated 1 M KOH. The glass carbon  
 electrode (GCE), graphite rod and Hg/HgO were selected as  
 working, counter and reference electrode, respectively. All the  
 potentials collected in this work were calibrated against  
 reversible hydrogen electrode (RHE), using Pt foil as the  
 working electrode and Pt wire as the counter electrode [36].  
 Therefore, the potentials can be obtained by the equation of  $E$   
 ( $\text{V vs. RHE}$ ) =  $E(\text{Hg/HgO}) + 0.932$ . The electrochemical  
 impedance spectroscopy (EIS) measurement was performed  
 within the frequency range from 100 kHz to 0.1 Hz at a potential  
 corresponding to the current density of  $10 \text{ mA cm}^{-2}$  [37]. The  
 cycle voltammogram (CV) curves were tested in 1 M KOH in the  
 non-Faradic region with scanning rate of 2, 4, 6, 8, 10 and 12  
 $\text{mV s}^{-1}$ . Double layer capacity ( $C_{dl}$ ) could be obtained by plotting  
 the current difference of the CV curves. Therefore, the  
 electrochemical active surface area (ECSA) was determined by  
 the equation of  $\text{ECSA} = C_{dl} / C_s \cdot S$ , where  $C_s$  is the specific  
 capacitance (herein  $0.04 \text{ mF cm}^{-2}$ ), and  $S$  is the surface  
 geometric area of the electrode [38].

## 3. Results and Discussion

### 3.1. Structural characterization of CoRu@N-CNTs

The synthesis route of CoRu@N-CNTs is schematically  
 illustrated in Scheme 1. During the hydrothermal process, the  
 as-formed CoRu nanoparticles were grafted on the surface of  
 fullerene, which was subsequently cracked into pieces of bowl-  
 like carbon fragments and emerged to N-doped CNTs in the  
 presence of melamine in the following annealing step [39]. From  
 the SEM and TEM images shown in Fig. 1a and 1b, it can be  
 found a plenty of CNTs decorated with metal nanoparticles. To  
 further clarify the structure of CoRu@N-CNTs, high-resolution  
 TEM (HRTEM) images were collected as displayed in Fig. 1c.  
 Clearly, the CoRu nanoparticles were distributed both on the  
 surface and inner wall of CNTs. The crystal lattice fringe of  
 $0.223 \text{ nm}$  (Fig. 1d) and  $0.207 \text{ nm}$  (Fig. 1e) could be assigned to  
 the (100) and (111) facets of CoRu alloy, respectively [40]. While  
 in the absence of  $\text{C}_{60}(\text{OH})_n$ , the CoRu nanoparticles were  
 embedded on the planar N-doped carbon matrix in CoRu@NC  
 (Fig. S1). As for Co@N-CNTs, the Co nanoparticles were mainly  
 enwrapped inside the CNTs (Fig. S2). Whereas in the absence  
 of Co precursor,  $\text{C}_{60}(\text{OH})_n$  and melamine were difficult to  
 transform to CNTs [23], resulting in a N-doped carbon  
 substrate decorated with Ru nanoparticles in Ru@NC (Fig. S3).  
 Therefore, it was Co that catalytically promote the  $\text{C}_{60}(\text{OH})_n$   
 together with melamine to generate N-doped CNTs in CoRu@N-  
 CNTs. In this case, Co nanoparticles were in a large proportion  
 encapsulated inside the CNTs while Ru was decorated on the  
 surface of CNTs, as demonstrated by the energy dispersive X-  
 ray spectroscopy (EDS) mapping of CoRu@N-CNTs (Fig. 1f).  
 As a result, CNTs served as electron collector that accelerate  
 the charge communication between the inner Co and outer Ru  
 to boost the HER activity.



1  
2 **Figure 1.** Structure characterization of CoRu@N-CNTs. (a) SEM, (b) TEM, (c), (d) and (e) HRTEM, (f) the corresponding elemental mapping of Co, Ru, O, C and  
3 N for CoRu@N-CNTs. Scale bar in (a-f): 1  $\mu\text{m}$ , 200 nm, 10 nm, 2 nm, 2 nm, 100 nm, respectively.

4 The crystal phase structure of CoRu@N-CNTs was then  
5 investigated by XRD. As can be seen from Fig. 2a, the  
6 diffraction peaks at 44.2°, 51.5° and 75.8° for Co@N-CNTs can  
7 be well indexed to the (111), (200) and (220) facets of Co with a  
8 face-centered cubic crystal structure (PDF #15-0806) [40],  
9 respectively. And the peaks at 38.4°, 42.2° and 44.0° in Ru@NC  
10 were attributed to the (100), (002) and (101) crystal lattices of  
11 hexagonal Ru (PDF#06-0663) [36], respectively. Fascinatingly,  
12 only a broadened peak around 44.0° assigned to the CoRu alloy  
13 (PDF#65-8975) with a slight upshift relative to Co@N-CNTs and  
14 Ru@NC was observed for CoRu@N-CNTs, probably owing to  
15 the strong electronic communication between Co and Ru within

the catalyst. Similar situation was also presented in CoRu@NC.  
Besides, the broad signal around 26° could be assigned to the  
graphitic carbon. Raman spectroscopy was also conducted to  
further explore the microstructure of CoRu@N-CNTs. As  
displayed in Fig. 2b, the D band (1345  $\text{cm}^{-1}$ ) and G band (1586  
 $\text{cm}^{-1}$ ) can be observed apparently [41], indicating the  
coexistence of disordered and graphitic carbon in the substrate.  
The integrated intensity ratio ( $I_D/I_G$ ) were determined to be 1.08,  
0.85, 0.98, 0.87 for CoRu@N-CNTs, CoRu@NC, Co@N-CNTs  
and Ru@NC respectively, indicative of a higher degree of  
defects in CoRu@N-CNTs.

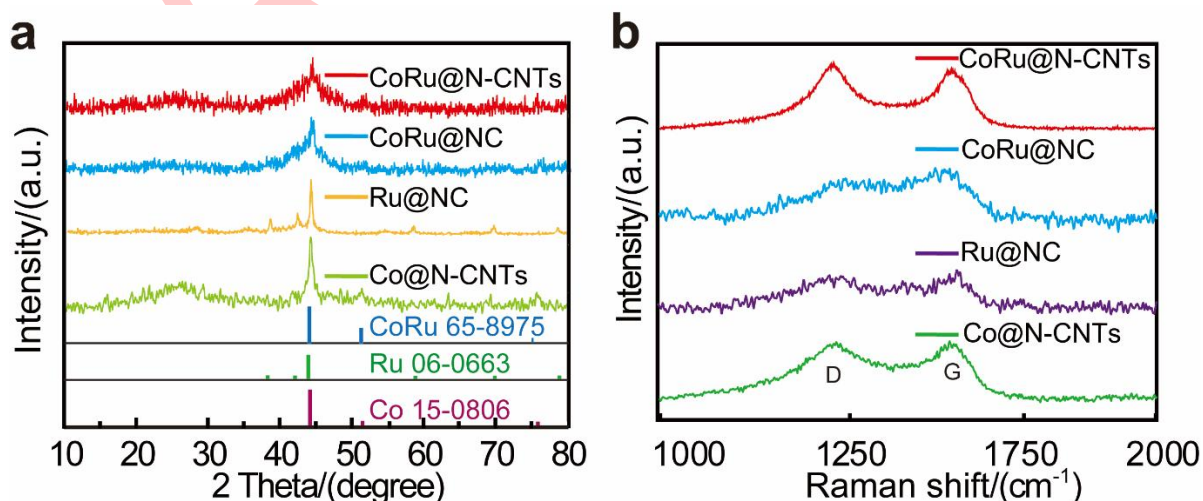
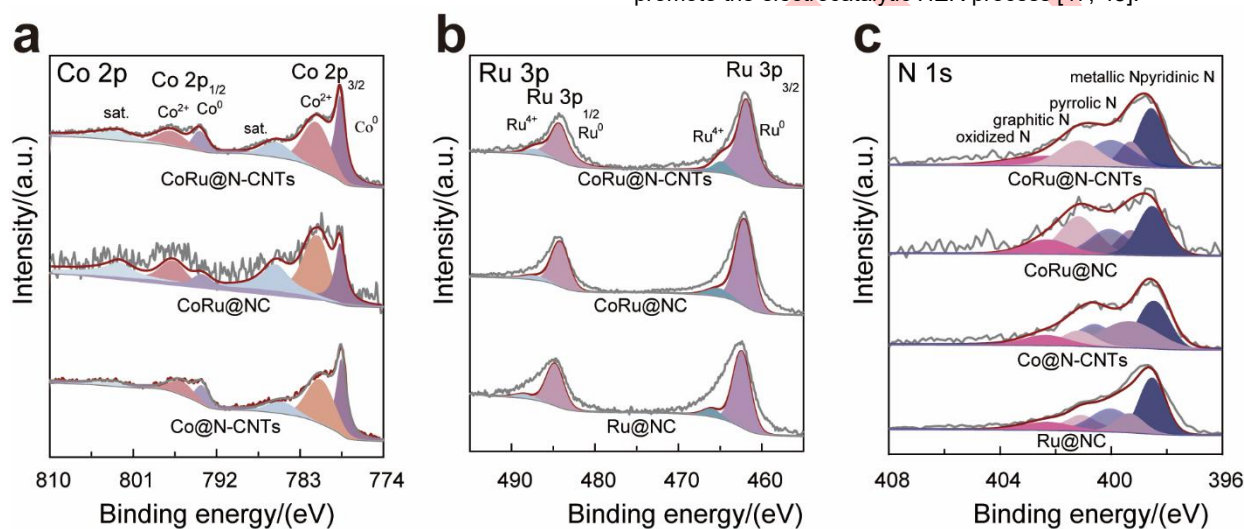


**Figure 2.** (a) XRD pattern and (b) Raman spectra of CoRu@N-CNTs, CoRu@NC, Ru@NC and Co@N-CNTs.

1 XPS was employed to examine the chemical states and  
 2 surface element distribution of the samples. In line with the EDS  
 3 results, the survey spectra demonstrated the existence of C, N,  
 4 O, Co, and Ru elements in CoRu@N-CNTs (Fig. S4 and Table  
 5 S1). The lack of Cl element excluded the contribution to  
 6 electrochemical process (Fig. S5). The high-resolution spectra of  
 7 Co 2p was displayed in Fig. 3a. Two peaks, corresponding to Co  
 8 2p<sub>3/2</sub> and Co 2p<sub>1/2</sub> of metallic Co (Co<sup>0</sup>), respectively, at 778.67  
 9 eV and 793.79 eV were observed in the spectrum of CoRu@N-  
 10 CNTs. While the Co<sup>2+</sup> is responsible for the peaks at 781.21 eV  
 11 (Co 2p<sub>3/2</sub>) and 796.73 eV (Co 2p<sub>1/2</sub>), and the set of peaks at  
 12 802.6 eV and 785.55 eV are satellite peaks [42, 43]. Fig. 3b  
 13 displayed the high-resolution spectrum of Ru 3p. Two distinct  
 14 peak groups were visible for CoRu@N-CNTs. The peaks located  
 15 at 461.87 eV and 484.27 eV could be assigned to the 3p<sub>3/2</sub> and

3p<sub>1/2</sub> of Ru, corresponding to metallic Ru. While another set of  
 peaks at 464.81 eV and 487.21 eV were responsible for oxidized  
 Ru species [44, 45]. It is worth noting that the Co 2p peaks in  
 CoRu@N-CNTs upshifted to the high binding energy meanwhile  
 the Ru 3p downshifted compared with those of the Co@N-CNTs  
 and Ru@NC counterparts, indicating a charge transfer occurred  
 between Co and Ru in CoRu@N-CNTs, which was beneficial for  
 the electrochemical reactions. The high-resolution N 1s  
 spectrum of CoRu@N-CNTs could be deconvoluted into five  
 parts (Fig. 3c), including the pyridinic N (398.56 eV), metallic N  
 (399.3 eV), pyrrolic N (400.00 eV), graphitic N (401.14 eV) and  
 oxidized N (402.5 eV) [38, 46]. The presence of M-N (M = Co,  
 Ru) species suggested that N doped in the carbon nanotubes  
 could anchor metal atoms, favoring the formation of diatomic  
 sites. Notably, the pyridinic N can serve as active sites to  
 promote the electrocatalytic HER process [47, 48].



32 **Figure 3.** High-resolution XPS spectra for (a) Co 2 p of CoRu@N-CNTs, CoRu@NC and Co@N-CNTs; (b) Ru 3 p of CoRu@N-CNTs, CoRu@NC and Ru@NC;  
 33 (c) N 1 s of CoRu@N-CNTs, CoRu@NC, Ru@NC and Co@N-CNTs.  
 34

### 35 3.2. Electrocatalytic performance for CoRu@N-CNTs

36 To evaluate the electrocatalytic performance of CoRu@N-  
 37 CNTs, HER measurements were conducted in Ar-saturated 1 M  
 38 KOH with a typical three-electrode system. For comparison,  
 39 CoRu@NC, Co@N-CNTs, Ru@NC and commercial Pt/C were  
 40 selected as references. To be accurate, the reference electrode  
 41 was calibrated against RHE in H<sub>2</sub>-saturated 1 M KOH media  
 42 before all the tests (Fig. S6). Firstly, the HER activity was  
 43 assessed using linear sweep voltammetry (LSV) with 85% iR-  
 44 corrections. As shown in Fig. 4a, the CoRu@N-CNTs exhibited  
 45 an outstanding electrocatalytic activity among all the samples.  
 46 To achieve a current density of 10 mA cm<sup>-2</sup>, the CoRu@N-CNTs  
 47 merely required an overpotential ( $\eta_{10}$ ) of 19 mV, much superior  
 48 to CoRu@NC (45 mV), Ru@NC (39 mV), Co@N-CNTs (219 mV)  
 49 and even the commercial benchmark 20% Pt/C (55 mV). The  
 50 HER kinetics was then assessed by Tafel plot shown in Fig. 4b.  
 51 Particularly, the CoRu@N-CNTs displayed a Tafel slope of  
 52 26.19 mV dec<sup>-1</sup>, much smaller than that of CoRu@NC (65.84  
 53 mV dec<sup>-1</sup>), Ru@NC (62.41 mV dec<sup>-1</sup>), Co@N-CNTs (174.08 mV  
 54 dec<sup>-1</sup>), and the commercial benchmark 20% Pt/C (94.16 mV dec<sup>-1</sup>).  
 55 indicating a favorable electrochemical reaction kinetics of

CoRu@N-CNTs [40, 46]. The small Tafel slope of CoRu@N-  
 CNTs suggested that the rate-limiting step is the recombination  
 of chemical adsorbed hydrogen and the HER over the catalysts  
 follow the Volmer-Tafel mechanism [49, 50]. The histograms  
 depicted in Fig. 4c demonstrated the superior catalytic activity  
 of CoRu@N-CNTs and its faster reaction kinetics for the HER.  
 In addition, the charge transfer kinetics of CoRu@N-CNTs,  
 CoRu@NC, Ru@NC, Co@N-CNTs and the commercial  
 benchmark 20% Pt/C were investigated by EIS measurement  
 (Fig. 4d). The charge transfer resistance ( $R_{ct}$ ) obtained from the  
 semicircle in the low-frequency region of the Nyquist plot is  
 related to the electrocatalytic kinetics at the interface between  
 the electrocatalyst and electrolyte, and a smaller value  
 corresponds to a faster electron transfer. Compared to  
 CoRu@NC ( $R_{ct} = 12.51 \Omega$ ), Co@N-CNTs ( $R_{ct} = 28.22 \Omega$ ),  
 Ru@NC ( $R_{ct} = 11.15 \Omega$ ) and Pt/C ( $R_{ct} = 25.18 \Omega$ ), CoRu@N-CNTs  
 possessed the smallest  $R_{ct}$  value of 7.24  $\Omega$ , indicative of the  
 fastest reaction rate. To unravel the intrinsic activity of  
 CoRu@N-CNTs, the  $C_{dl}$  were obtained by scanning CV curves  
 in the non-faradic region (Fig. S7), which is positively  
 proportional to ECSA [21, 27]. As shown in Fig. 4e, CoRu@N-  
 CNTs delivers a significantly larger  $C_{dl}$  value (103.9 mF cm<sup>-2</sup>)

1 than that of CoRu@NC ( $49.8 \text{ mF cm}^{-2}$ ), Ru@NC ( $94.2 \text{ mF cm}^{-2}$ ),  
 2 Co@N-CNTs ( $75.1 \text{ mF cm}^{-2}$ ) and Pt/C ( $10.2 \text{ mF cm}^{-2}$ ).  
 3 Moreover, the ECSA-normalized LSV further confirmed the  
 4 excellent intrinsic activity of CoRu@N-CNTs (Fig. S8). To further  
 5 evaluate the long-term stability of the CoRu@N-CNTs, the  
 6 chronopotentiometry were also conducted as shown in Fig. 4f. It  
 7 can be seen that the current density remains almost unchanged

after 50 h at the current density of  $15 \text{ mA cm}^{-2}$ . In addition, the  
 LSV curve after continuously scanning by CV for 2000 cycles  
 displayed negligible decay (inset of Fig. 4f). Besides, the HER  
 performance of CoRu@N-CNTs surpassed most of the recently  
 reported Co/Ru-based HER electrocatalysts (Fig. 4g and Table  
 S2).

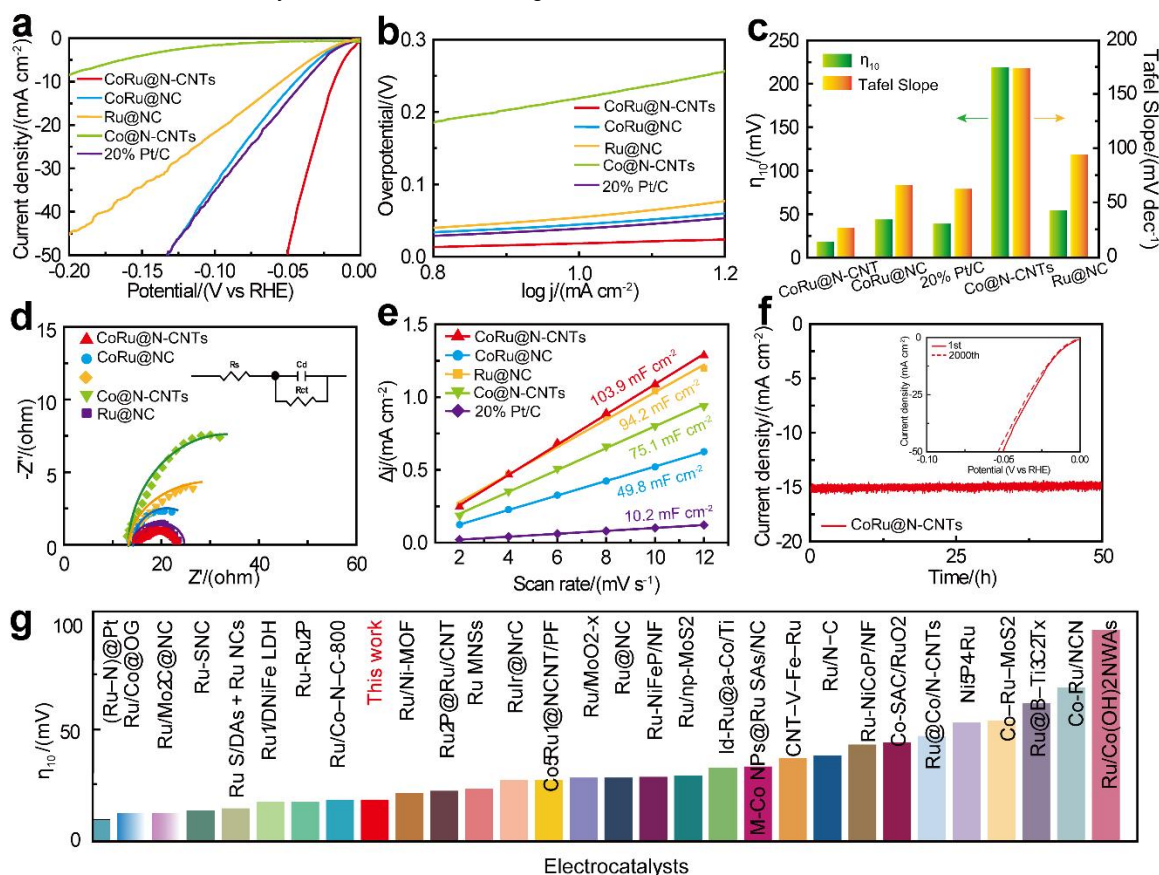


**Figure 4.** Electrochemical HER performance in 1.0 M KOH. (a) The LSV curves, (b) Tafel plots, (c) the histograms of overpotential and Tafel slopes, (d) Nyquist plot and (e) current density difference against scan rate of CoRu@N-CNTs, CoRu@NC, Ru@NC, Co@N-CNTs and the commercial benchmark 20% Pt/C. (f) Long-term chronoamperometric test of CoRu@N-CNTs, inset showing the LSV curves of CoRu@N-CNTs before (solid) and after (dashed) 2000 CV cycles. (g) Performance comparison of CoRu@N-CNTs with recently-reported Co/Ru-based HER electrocatalysts in 1.0 M KOH.

## 4. Conclusion

In summary, a Co and Ru bimetallic electrocatalyst consisting of CoRu nanoalloy uniformly distributed on N-CNTs, were successfully prepared through hydrothermal reaction of  $\text{Ru}^{3+}$ ,  $\text{C}_{60}(\text{OH})_n$  and melamine in the presence of  $\text{Co}^{2+}$ . The as-obtained CoRu@N-CNTs exhibited superior electrocatalytic HER activity in alkaline condition, *i.e.*, it only needed an overpotential 19 mV to reach a current density of  $10 \text{ mA cm}^{-2}$ , with a Tafel slope of  $26.19 \text{ mV dec}^{-1}$  in 1 M KOH and long-term durability. The enhanced electrocatalytic HER performance of CoRu@N-CNTs could be attributed to the following aspects: (1) The electronic communication between Ru and Co sites induced a synergistically electrocatalytic effect, and thus improving the charge distribution of CoRu@N-CNTs, which in turn facilitates

the electrocatalytic HER process; (2) The N-CNTs not only served as electron collector, accelerating the charge transfer between the catalyst and electrolyte, but also provide a tubular channel, which is beneficial to the mass and charge transportation; (3) The synergistic electronic metal-support interaction (EMSI) between the pyridinic N and CoRu bimetallic sites improved the electronic structure of CoRu@N-CNTs, thus boosting the electrocatalyst HER performance. This work provides a new idea for the design and construction of novel and efficient electrocatalysts in the field of energy storage and conversion.

## Acknowledgements

1 This work was supported by the National Natural Science  
2 Foundation of China (No. 52072226, U22A20144), Key  
3 Research and Development Program of Shaanxi (2024GX-  
4 YBXM-466), Science and Technology Program of Xi'an, China  
5 (22GXFW0013), and Science and Technology Program of  
6 Weiyang District of Xi'an, China (202315).

## 7 References

- 8 [1] Qiao M, Wang Y, Wang Q, Hu G, Mamat X, Zhang S, Wang S.  
9 Hierarchically Ordered Porous Carbon with Atomically Dispersed Fe<sub>n</sub>  
10 for Ultraefficient Oxygen Reduction Reaction in Proton-Exchange  
11 Membrane Fuel Cells[J]. *Angew. Chem. Int. Ed.*, 2020, 59(7): 2688-  
12 2694.
- 13 [2] Wang J, Cui W, Liu Q, Xing Z, Asiri AM, Sun X. Recent Progress in  
14 Cobalt-Based Heterogeneous Catalysts for Electrochemical Water  
15 Splitting[J]. *Adv. Mater.*, 2016, 28(2): 215-230.
- 16 [3] Hodges A, Hoang AL, Tsekouras G, Wagner K, Lee C-Y, Swiegers GF,  
17 Wallace GG. A High-Performance Capillary-Fed Electrolysis Cell  
18 Promises More Cost-Competitive Renewable Hydrogen[J]. *Nat.*  
19 *Commun.*, 2022, 13(1): 1304.
- 20 [4] Chu C, Huang D, Gupta S, Weon S, Niu J, Stavitski E, Muhich C, Kim  
21 J-H. Neighboring Pd Single Atoms Surpass Isolated Single Atoms for  
22 Selective Hydrodehalogenation Catalysis[J]. *Nat. Commun.*, 2021,  
23 12(1): 5179.
- 24 [5] Kang J, Qiu X, Hu Q, Zhong J, Gao X, Huang R, Wan C, Liu L-M,  
25 Duan X, Guo L. Valence Oscillation and Dynamic Active Sites in  
26 Monolayer NiCo Hydroxides for Water Oxidation[J]. *Nat. Catal.*, 2021,  
27 4(12): 1050-1058.
- 28 [6] Gao T, Li X, Chen X, Zhou C, Yue Q, Yuan H, Xiao D. Ultra-Fast  
29 Preparing Carbon Nanotube-Supported Trimetallic Ni, Ru, Fe  
30 Heterostructures as Robust Bifunctional Electrocatalysts for Overall  
31 Water Splitting[J]. *Chem. Eng. J.*, 2021, 424: 130416.
- 32 [7] Wang T-J, Jiang Y-C, He J-W, Li F-M, Ding Y, Chen P, Chen Y.  
33 Porous Palladium Phosphide Nanotubes for Formic Acid  
34 Electrooxidation[J]. *Carbon Energy*, 2022, 4(3): 283-293.
- 35 [8] Jiang W-J, Tang T, Zhang Y, Hu J-S. Synergistic Modulation of Non-  
36 Precious-Metal Electrocatalysts for Advanced Water Splitting[J]. *Acc.*  
37 *Chem. Res.*, 2020, 53(6): 1111-1123.
- 38 [9] Huang C, Ouyang T, Zou Y, Li N, Liu Z-Q. Ultrathin NiCo<sub>2</sub>p  
39 Nanosheets Strongly Coupled with Cnts as Efficient and Robust  
40 Electrocatalysts for Overall Water Splitting[J]. *J. Mater. Chem. A*, 2018,  
41 6(17): 7420-7427.
- 42 [10] Olabi AG, Abdelkareem MA. Renewable Energy and Climate Change[J].  
43 *Renew. Sus. Energ. Rev.*, 2022, 158: 112111.
- 44 [11] Wang X, Zhao L, Li X, Liu Y, Wang Y, Yao Q, Xie J, Xue Q, Yan Z,  
45 Yuan X, Xing W. Atomic-Precision Pt<sub>6</sub> Nanoclusters for Enhanced  
46 Hydrogen Electro-Oxidation[J]. *Nat. Commun.*, 2022, 13(1): 1596.
- 47 [12] Zaman S, Huang L, Douka AI, Yang H, You B, Xia BY. Oxygen  
48 Reduction Electrocatalysts toward Practical Fuel Cells: Progress and  
49 Perspectives[J]. *Angew. Chem. Int. Ed.*, 2021, 60(33): 17832-17852.
- 50 [13] Chen H, Zhang B, Liang X, Zou X. Light Alloying Element-Regulated  
51 Noble Metal Catalysts for Energy-Related Applications[J]. *Chinese J.*  
52 *Catal.*, 2022, 43(3): 611-635.
- 53 [14] Sun Y, Xue Z, Liu Q, Jia Y, Li Y, Liu K, Lin Y, Liu M, Li G, Su C-Y.  
54 Modulating Electronic Structure of Metal-Organic Frameworks by  
Introducing Atomically Dispersed Ru for Efficient Hydrogen Evolution[J].  
*Nat. Commun.*, 2021, 12(1): 1369.
- [15] Clay C, Haq S, Hodgson A. Intact and Dissociative Adsorption of Water  
on Ru(0001)[J]. *Chem. Phys. Lett.*, 2004, 388(1): 89-93.
- [16] Cao X, Huo J, Li L, Qu J, Zhao Y, Chen W, Liu C, Liu H, Wang G.  
Recent Advances in Engineered Ru-Based Electrocatalysts for the  
Hydrogen/Oxygen Conversion Reactions[J]. *Adv. Energy Mater.*, 2022,  
12(41): 2202119.
- [17] Liu Z, Zeng L, Yu J, Yang L, Zhang J, Zhang X, Han F, Zhao L, Li X,  
Liu H, Zhou W. Charge Redistribution of Ru Nanoclusters on Co<sub>3</sub>O<sub>4</sub>  
Porous Nanowire Via the Oxygen Regulation for Enhanced Hydrogen  
Evolution Reaction[J]. *Nano Energy*, 2021, 85: 105940.
- [18] Wang Y, Luo W, Li H, Cheng C. Ultrafine Ru Nanoclusters Supported  
on N/S Doped Macroporous Carbon Spheres for Efficient Hydrogen  
Evolution Reaction[J]. *Nanoscale Adv.*, 2021, 3(17): 5068-5074.
- [19] Wu Y-L, Li X, Wei Y-S, Fu Z, Wei W, Wu X-T, Zhu Q-L, Xu Q. Ordered  
Macroporous Superstructure of Nitrogen-Doped Nanoporous Carbon  
Implanted with Ultrafine Ru Nanoclusters for Efficient Ph-Universal  
Hydrogen Evolution Reaction[J]. *Adv. Mater.*, 2021, 33(12): 2006965.
- [20] Zhang X, Ma J, Yan R, Cheng W, Zheng J, Jin B. Pt-  
Ru/Polyaniline/Carbon Nanotube Composites with Three-Layer Tubular  
Structure for Efficient Methanol Oxidation[J]. *J. Alloy. Compd*, 2021,  
867: 159017.
- [21] Zhai P, Xia M, Wu Y, Zhang G, Gao J, Zhang B, Cao S, Zhang Y, Li Z,  
Fan Z, Wang C, Zhang X, Miller JT, Sun L, Hou J. Engineering Single-  
Atomic Ruthenium Catalytic Sites on Defective Nickel-Iron Layered  
Double Hydroxide for Overall Water Splitting[J]. *Nat. Commun.*, 2021,  
12(1): 4587.
- [22] Han X, Li Y, Wang X, Dong J, Li H, Yin S, Xia J. Ru Anchored on  
Co(OH)<sub>2</sub> Nanowire Arrays as Highly Effective Electrocatalyst for Full  
Water Splitting[J]. *Int. J. Hydrogen Energ.*, 2024, 51: 769-776.
- [23] Liu Z, Yang X, Hu G, Feng L. Ru Nanoclusters Coupled on Co/N-  
Doped Carbon Nanotubes Efficiently Catalyzed the Hydrogen Evolution  
Reaction[J]. *ACS Sustain. Chem. Eng.*, 2020, 8(24): 9136-9144.
- [24] Shah K, Dai R, Mateen M, Hassan Z, Zhuang Z, Liu C, Israr M, Cheong  
W-C, Hu B, Tu R, Zhang C, Chen X, Peng Q, Chen C, Li Y. Cobalt  
Single Atom Incorporated in Ruthenium Oxide Sphere: A Robust  
Bifunctional Electrocatalyst for Her and Oer[J]. *Angew. Chem. Int. Ed.*,  
2022, 61(4): e202114951.
- [25] Martínez-Séptimo A, Valenzuela MA, Del Angel P, González-Huerta  
RdG. IrRuOx/TiO<sub>2</sub> a Stable Electrocatalyst for the Oxygen Evolution  
Reaction in Acidic Media[J]. *Int. J. Hydrogen Energ.*, 2021, 46(51):  
25918-25928.
- [26] Li G, Jang H, Liu S, Li Z, Kim MG, Qin Q, Liu X, Cho J. The Synergistic  
Effect of Hf-O-Ru Bonds and Oxygen Vacancies in Ru/HfO<sub>2</sub> for  
Enhanced Hydrogen Evolution[J]. *Nat. Commun.*, 2022, 13(1): 1270.
- [27] Feng W, Feng Y, Chen J, Wang H, Hu Y, Luo T, Yuan C, Cao L, Feng  
L, Huang J. Interfacial Electronic Engineering of Ru/Ferri Nanoparticles  
as Efficient Trifunctional Electrocatalyst for Overall Water Splitting and  
Zn-Air Battery[J]. *Chem. Eng. J.*, 2022, 437: 135456.
- [28] Lin S-Y, Chen Y-P, Cao Y, Zhang L, Feng J-J, Wang A-J. Aminouracil-  
Assisted Synthesis of Cofe Decorated Bougainvillea-Like N-Doped  
Carbon Nanoflowers for Boosting Zn-Air Battery and Water  
Electrolysis[J]. *J. Power Sources*, 2022, 521: 230926.
- [29] Song H, Wu M, Tang Z, Tse JS, Yang B, Lu S. Single Atom Ruthenium-  
Doped Cop/Cds Nanosheets Via Splicing of Carbon-Dots for Robust

- 1 Hydrogen Production[J]. *Angew. Chem. Int. Ed.*, 2021, 60(13): 7234-  
2 7244.
- 3 [30] Kumar A, Bui VQ, Lee J, Wang L, Jadhav AR, Liu X, Shao X, Liu Y, Yu  
4 J, Hwang Y, Bui HTD, Ajmal S, Kim MG, Kim S-G, Park G-S, Kawazoe  
5 Y, Lee H. Moving Beyond Bimetallic-Alloy to Single-Atom Dimer  
6 Atomic-Interface for All-Ph Hydrogen Evolution[J]. *Nat. Commun.*, 2021,  
7 12(1): 6766.
- 8 [31] Lu Z, Wang B, Hu Y, Liu W, Zhao Y, Yang R, Li Z, Luo J, Chi B, Jiang Z,  
9 Li M, Mu S, Liao S, Zhang J, Sun X. An Isolated Zinc-Cobalt Atomic  
10 Pair for Highly Active and Durable Oxygen Reduction[J]. *Angew. Chem.*  
11 *Int. Ed.*, 2019, 58(9): 2622-2626.
- 12 [32] Bai L, Hsu C-S, Alexander DTL, Chen HM, Hu X. Double-Atom  
13 Catalysts as a Molecular Platform for Heterogeneous Oxygen Evolution  
14 Electrocatalysis[J]. *Nature Energy*, 2021, 6(11): 1054-1066.
- 15 [33] Liu D, Zhao Y, Wu C, Xu W, Xi S, Chen M, Yang L, Zhou Y, He Q, Li X,  
16 Ge B, Song L, Jiang J, Yan Q. Triggering Electronic Coupling between  
17 Neighboring Hetero-Diatomic Metal Sites Promotes Hydrogen Evolution  
18 Reaction Kinetics[J]. *Nano Energy*, 2022, 98: 107296.
- 19 [34] Li J, Hou C, Chen C, Ma W, Li Q, Hu L, Lv X, Dang J. Collaborative  
20 Interface Optimization Strategy Guided Ultrafine Ruco and Mxene  
21 Heterostructure Electrocatalysts for Efficient Overall Water Splitting[J].  
22 *ACS Nano*, 2023, 17(11): 10947-10957.
- 23 [35] Su K, Yang S, Yang A, Guo Y, Liu B, Zhu J, Tang Y, Qiu X.  
24 Customizing the Anisotropic Electronic States of Janus-Distributive  
25 Fen<sub>4</sub> and Nin<sub>4</sub> Dual-Atom Sites for Reversible Oxygen  
26 Electrocatalysis[J]. *Appl. Catal. B-Environ.*, 2023, 331: 122694.
- 27 [36] Luo T, Huang J, Hu Y, Yuan C, Chen J, Cao L, Kajiyoshi K, Liu Y, Zhao  
28 Y, Li Z, Feng Y. Fullerene Lattice-Confined Ru Nanoparticles and  
29 Single Atoms Synergistically Boost Electrocatalytic Hydrogen Evolution  
30 Reaction[J]. *Adv. Funct. Mater.*, 2023, 33(12): 2213058.
- 31 [37] Wei C, Rao RR, Peng J, Huang B, Stephens IEL, Risch M, Xu ZJ,  
32 Shao-Horn Y. Recommended Practices and Benchmark Activity for  
33 Hydrogen and Oxygen Electrocatalysis in Water Splitting and Fuel  
34 Cells[J]. *Adv. Mater.*, 2019, 31(31): 1806296.
- 35 [38] Chen J, Huang J, Wang R, Feng W, Wang H, Luo T, Hu Y, Yuan C,  
36 Feng L, Cao L, Kajiyoshi K, He C, Liu Y, Li Z, Feng Y. Atomic  
37 Ruthenium Coordinated with Chlorine and Nitrogen as Efficient and  
38 Multifunctional Electrocatalyst for Overall Water Splitting and  
39 Rechargeable Zinc-Air Battery[J]. *Chem. Eng. J.*, 2022, 441: 136078.
- 40 [39] Feng Y, Li X, Liu Q, Zhu W, Huo X, Gao M, Liu W, Wang Y, Wei Y.  
41 Fullerene-Derived Nanocomposite as an Efficient Electrocatalyst for  
42 Overall Water Splitting and Zn-Air Battery[J]. *Mater. Chem. Front.*,  
43 2023, 7(24): 6446-6462.
- 44 [40] Chen J, Huang J, Zhao Y, Cao L, Kajiyoshi K, Liu Y, Li Z, Feng Y.  
45 Enhancing the Electronic Metal-Support Interaction of Coru Alloy and  
46 Pyridinic N for Electrocatalytic Ph-Universal Hydrogen Evolution  
47 Reaction[J]. *Chem. Eng. J.*, 2022, 450: 138026.
- 48 [41] Duan S, Han G, Su Y, Zhang X, Liu Y, Wu X, Li B. Magnetic Co@G-  
49 C<sub>3</sub>n<sub>4</sub> Core-Shells on Rgo Sheets for Momentum Transfer with  
50 Catalytic Activity toward Continuous-Flow Hydrogen Generation[J].  
51 *Langmuir*, 2016, 32(25): 6272-6281.
- 52 [42] Zhang F, Zhu Y, Chen Y, Lu Y, Lin Q, Zhang L, Tao S, Zhang X, Wang  
53 H. Ruco Alloy Bimodal Nanoparticles Embedded in N-Doped Carbon: A  
54 Superior Ph-Universal Electrocatalyst Outperforms Benchmark Pt for  
55 the Hydrogen Evolution Reaction[J]. *J. Mater. Chem. A*, 2020, 8(25):  
56 12810-12820.
- [43] Zhang M, Wang J, Zhang Y, Ye L, Gong Y. Ultrafine Coru Alloy  
Nanoparticles in Situ Embedded in Co<sub>4</sub>n Porous Nanosheets as High-  
Efficient Hydrogen Evolution Electrocatalysts[J]. *Dalton Trans.*, 2021,  
50(8): 2973-2980.
- [44] Chen J, Ha Y, Wang R, Liu Y, Xu H, Shang B, Wu R, Pan H. Inner Co  
Synergizing Outer Ru Supported on Carbon Nanotubes for Efficient Ph-  
Universal Hydrogen Evolution Catalysis[J]. *Nano-Micro Lett.*, 2022,  
14(1): 186.
- [45] Cao D, Wang J, Xu H, Cheng D. Construction of Dual-Site Atomically  
Dispersed Electrocatalysts with Ru-C<sub>5</sub> Single Atoms and Ru-O<sub>4</sub>  
Nanoclusters for Accelerated Alkali Hydrogen Evolution[J]. *Small*, 2021,  
17(31): 2101163.
- [46] Tiwari JN, Harzandi AM, Ha M, Sultan S, Myung CW, Park HJ, Kim DY,  
Thangavel P, Singh AN, Sharma P, Chandrasekaran SS, Salehnia F,  
Jang J-W, Shin HS, Lee Z, Kim KS. High-Performance Hydrogen  
Evolution by Ru Single Atoms and Nitrided-Ru Nanoparticles Implanted  
on N-Doped Graphitic Sheet[J]. *Adv. Energy Mater.*, 2019, 9(26):  
1900931.
- [47] Zhao D, Sun K, Cheong W-C, Zheng L, Zhang C, Liu S, Cao X, Wu K,  
Pan Y, Zhuang Z, Hu B, Wang D, Peng Q, Chen C, Li Y. Synergistically  
Interactive Pyridinic-N-Mop Sites: Identified Active Centers for  
Enhanced Hydrogen Evolution in Alkaline Solution[J]. *Angew. Chem.*  
*Int. Ed.*, 2020, 59(23): 8982-8990.
- [48] Yu W, Huang H, Qin Y, Zhang D, Zhang Y, Liu K, Zhang Y, Lai J, Wang  
L. The Synergistic Effect of Pyrrolic-N and Pyridinic-N with Pt under  
Strong Metal-Support Interaction to Achieve High-Performance Alkaline  
Hydrogen Evolution[J]. *Adv. Energy Mater.*, 2022, 12(21): 2200110.
- [49] Chen Y, Ding R, Li J, Liu J. Highly Active Atomically Dispersed  
Platinum-Based Electrocatalyst for Hydrogen Evolution Reaction  
Achieved by Defect Anchoring Strategy[J]. *Appl. Catal. B-Environ.*,  
2022, 301: 120830.
- [50] Su P, Pei W, Wang X, Ma Y, Jiang Q, Liang J, Zhou S, Zhao J, Liu J,  
Lu GQ. Exceptional Electrochemical Her Performance with Enhanced  
Electron Transfer between Ru Nanoparticles and Single Atoms  
Dispersed on a Carbon Substrate[J]. *Angew. Chem. Int. Ed.*, 2021,  
60(29): 16044-16050.

# 氮掺杂碳纳米管上 Co 和 Ru 位点之间的电子通信促进碱性析氢反应

高梦婷<sup>a,#</sup>, 卫莹<sup>a,#</sup>, 霍雪萌<sup>a</sup>, 朱文洁<sup>a</sup>, 刘箐箐<sup>a</sup>, 强晋源<sup>a</sup>, 刘婉婉<sup>a</sup>, 王颖<sup>a</sup>, 李旭<sup>a</sup>, 黄剑锋<sup>a</sup>, 冯永强<sup>a\*</sup>

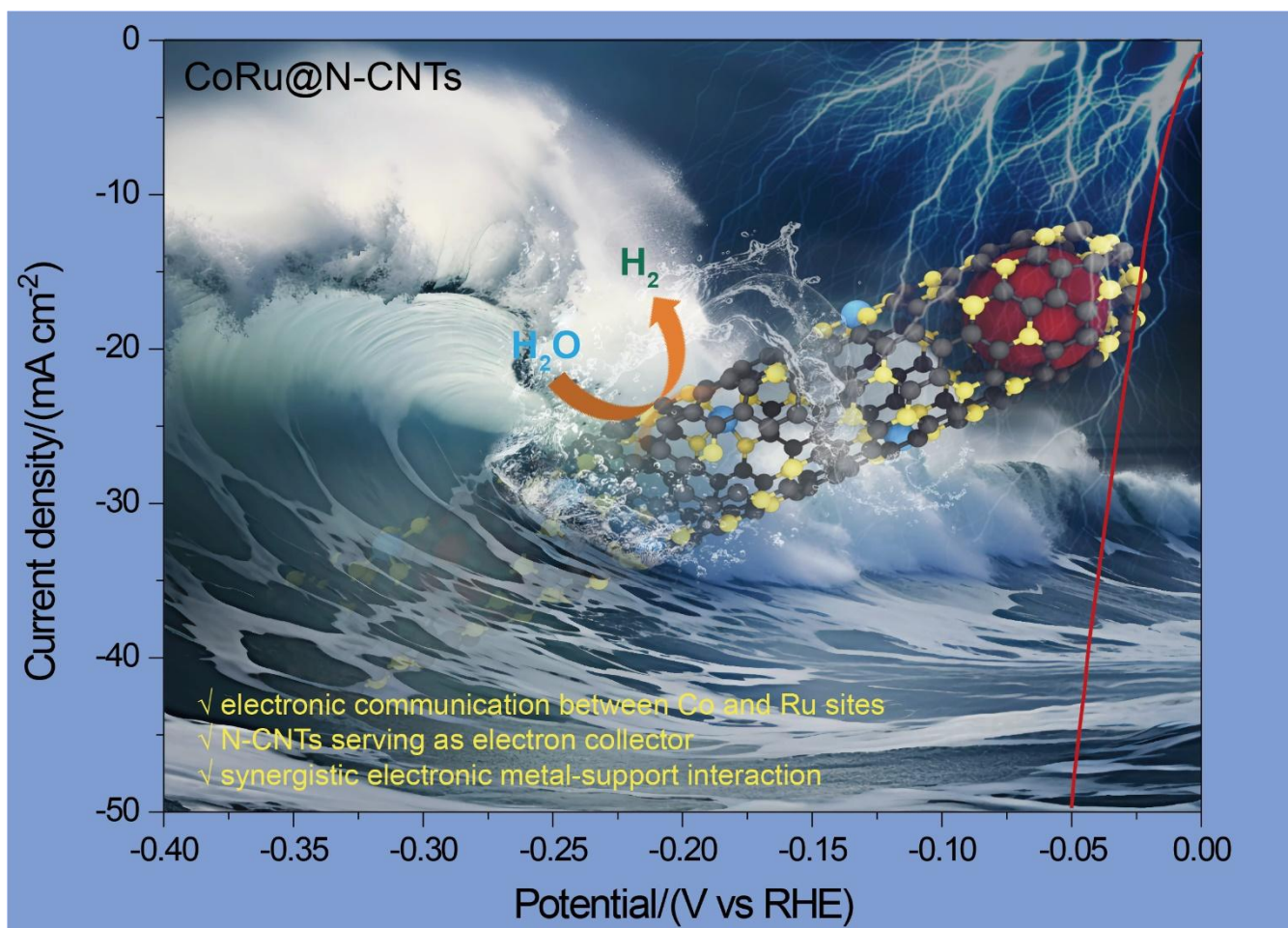
(a. 陕西科技大学, 材料科学与工程学院, 西安 710021)

**摘要:** 碱性电解水析氢反应(HER)作为获取绿色氢能源的重要途径具有广泛的研究意义和应用价值, 但其缓慢的电极反应动力学及较高的过电位需要高效稳定的催化剂来加速反应过程。目前商用的铂(Pt)基催化剂因高昂的成本限制了其规模化应用。设计高效、低过电位的非Pt电催化剂仍然是一个重大挑战。钌(Ru)基催化剂因具有类Pt的活性氢结合能而受到广泛关注。本文以富勒醇和三聚氰胺为基体原料, 与CoCl<sub>2</sub>和RuCl<sub>3</sub>在150 °C水热反应24 h, 随后在Ar/H<sub>2</sub>(5%)混合气氛下600 °C热解处理, 成功在氮掺杂碳纳米管(N-CNTs)上修饰了CoRu纳米合金, 制备了一种新型高效的Co, Ru双金属电催化剂。得益于Co和Ru位点之间的电子通信, 所得CoRu@N-CNTs具有优异的电催化HER活性。在1 M KOH水溶液达到10 mA cm<sup>-2</sup>的电流密度, 所需过电位仅为19 mV, 塔菲尔斜率为26.19 mV/dec<sup>-1</sup>, 优于基准Pt/C催化剂。本研究将为高效析氢电催化剂的设计与制造开辟一条新的道路, 有力推动电解水制氢技术在能源存储与转化领域的应用推广, 为我国“碳达峰与碳中和”战略目标的实施蓄势赋能。

**关键词:** 钴钌合金; 电催化剂; 水裂解; 析氢反应; 碳纳米管

1  
2

## For Table of Contents Only

3  
4  
5

ACCEPTED